Geophysical Research Letters

RESEARCH LETTER
10.1029/2018GL080006

Mesoscale Eddies Modulate Mixed Layer Depth Globally

Peter Gaube[1], **Dennis J. McGillicuddy Jr.**[2], **and Aurélie J. Moulin**[1]

[1]Woods Hole Oceanographic Institution, Woods Hole, MA, USA, [2]Applied Physics Laboratory, University of Washington, Seattle, WA, USA

Key Points:
- Anticyclonic and cyclonic eddies are observed to deepen and shoal the mixed layer, respectively
- The largest eddy-induced MLD anomalies are observed during the winter in regions of large eddy amplitude
- Observations reveal that larger MLD anomalies are more common in anticyclones versus cyclones

Supporting Information:
- Supporting Information S1
- Data Set S1

Correspondence to:
P. Gaube,
pgaube@apl.washington.edu

Citation:
Gaube, P., McGillicuddy Jr., D. J., & Moulin, A. J. (2019). Mesoscale eddies modulate mixed layer depth globally. *Geophysical Research Letters*, *46*, 1505–1512. https://doi.org/10.1029/2018GL080006

Received 18 AUG 2018
Accepted 3 DEC 2018
Accepted article online 6 DEC 2018
Published online 1 FEB 2019

Abstract Mesoscale eddies, energetic vortices covering nearly a third of the ocean surface at any one time, modulate the spatial and temporal evolution of the mixed layer. We present a global analysis of concurrent satellite observations of mesoscale eddies with hydrographic profiles by autonomous Argo floats, revealing rich geographic and seasonal variability in the influence of eddies on mixed layer depth. Anticyclones deepen the mixed layer depth, whereas cyclones thin it, with the magnitude of these eddy-induced mixed layer depth anomalies being largest in winter. Eddy-centric composite averages reveal that the largest anomalies occur at the eddy center and decrease with distance from the center. Furthermore, the extent to which eddies modulate mixed layer depth is linearly related to the sea surface height amplitude of the eddies. Finally, large eddy-mediated mixed layer depth anomalies are more common in anticyclones when compared to cyclones. We present candidate mechanisms for this observed asymmetry.

Plain Language Summary Mesoscale eddies, rotating bodies of water that can be hundreds of kilometers across and reach thousands of meters into the ocean interior, are found nearly everywhere in the ocean. These eddies are know to transport vast amounts of heat, salt, and ocean life across hundreds to thousands of kilometers. This study investigates how these eddies control the depth to which the surface of the ocean is mixed. Wind and the transfer of heat between the ocean and atmosphere are two of the primary ways in which the ocean surface is homogenized. The depth of this mixed layer, the mixed layer depth, is shown to be deeper in eddies that are warm, when compared to their surrounds, and shallower in cold eddies. We show that the stronger or more energetic the eddies are, the larger their influence is on mixed layer depth.

1. Introduction

The near-surface mixed layer is the conduit by which the atmosphere influences the ocean interior, and conversely, the ocean modulates fluxes into the atmosphere. In addition, primary production in the ocean is modulated by fluxes of nutrients and phytoplankton through the base of the mixed layer and the availability of light (Dawson et al., 2018; Frenger et al., 2018; Song et al., 2018). The fact that mesoscale eddies modulate the spatial and temporal evolution of the mixed layer has been known for decades (e.g., Klein et al., 1998). Targeted surveys have shown that the mixed layer depth (MLD) is deeper in anticyclonic eddies and shallower in cyclonic eddies (Dewar & Flierl, 1987; Joyce et al., 1981; Schmitt & Olson, 1985; Scott & Wang, 2005; The Ring Group, 1981; Vastano et al., 1980; Williams, 1988). More recently, a focused field study of eddies originating from the Leeuwin Current documented $O(100\ \mathrm{m})$ MLD anomalies associated with these coherent vortices (Waite et al., 2007).

With the advent of automated eddy identification and detection methods, coupled with hydrographic profiles collected from the global Argo float network, recent analysis has shown that the influence of eddies on MLD is ubiquitous and varies seasonally, with the largest eddy-induced MLD anomalies observed during the winter (Dufois et al., 2014, 2016; Gaube et al., 2013; Hausmann et al., 2017). In the Southern Ocean, the magnitude of eddy-induced MLD anomalies is largest in regions dominated by large energetic eddies (Hausmann et al., 2017). Furthermore, the work of Hausmann et al. (2017) revealed that the magnitude of eddy-mediated MLD perturbations were largest at the center of Southern Ocean eddies and decayed toward the eddy periphery. In the Southern Ocean this eddy-mediated MLD variability has been shown to generate enhanced iron flux in anticyclonic eddies (Song et al., 2018) that leads to elevated near-surface chlorophyll during the austral summer (Dawson et al., 2018; Frenger et al., 2018; Song et al., 2018). Using a global eddy-resolving simulation,

Dufois et al. (2016) showed that during the winter, nutrients from below the mixed layer were entrained into the interiors of anticyclones at higher rates when compared to cyclones and the areas outside of the influence of eddies, leading the authors to suggest eddy-mediated MLD perturbations as a mechanism by which elevated near-surface chlorophyll concentrations could be sustained in anticyclones. The extent to which eddies influence MLD globally, however, has not been documented.

2. Methodology and Data

Coherent mesoscale structures, defined here as mesoscale eddies, were identified and tracked in daily maps of sea level anomaly (SLA) computed by spatially high-pass filtering sea surface height fields distributed by Archiving, Validation and Interpretation of Satellite Oceanographic (AVISO) (Chelton, Schlax, & Samelson, 2011). Eddies were identified and tracked using a method that "grows" eddies from individual SLA extrema, in contrast to methods that identify eddies as closed contours of SLA (e.g., Chelton, Schlax, & Samelson, 2011). The eddy "growing" method has the advantage that it is computationally less expensive and can easily be extended to three dimensions. The eddy growing method is described in detail by Chelton and Schlax (2016) and builds on the work of Williams et al. (2011). Eddies were "grown" from individual SLA extrema (positive for anticyclones and negative for cyclones) by finding all neighboring pixels whose SLA values lie above a sequence of thresholds. The thresholds included checks to ensure the pixels are connected do not fall within the bounds of another eddy and do not exceed a maximum distance criteria. Thresholds were chosen by Chelton and Schlax (2016) to yield eddies with similar characteristics as those tracked using the closed contour method of Chelton, Gaube, et al. (2011). As described in Chelton, Gaube, et al. (2011), a minimum eddy life time of 4 weeks was used to eliminate the influence of ephemeral, or even "spurious" eddies perhaps resulting from artifacts of the interpolation procedure. In the supporting information we provide evidence that the choice of eddy data set does not significantly affect the results presented here.

The location of the eddy center is defined as the centroid of all points within the eddy. Eddy amplitude is computed as the difference between the magnitude of the extremum SLA value and the average of SLA over the pixels that define the outer perimeter of the eddy, hereafter called edge pixels. Rotational velocity, used to estimate eddy radius, is defined as the maximum geostrophic velocity computed along the edge pixels during all iterations of the "eddy growing" method. The SLA contour along which the maximum rotational velocity occurs defines the *speed core* of the eddy. The radius of a circle with area equal to that of the speed core defines the speed-based eddy radius L_s.

MLD estimates are derived from hydrographic profiles collected by the autonomous Argo float array (Holte et al., 2017). We use the density-based algorithm for MLD described in Holte and Talley (2009). The location of each individual Argo float profile was collocated with the nearest eddy center. The distance from the eddy center was normalized by the eddy radius L_s. Profiles within the distance $r \leq L_s$ from the eddy center were considered to be inside of the eddy. In the supporting information we show that the results presented here are not particularly sensitive to the choice of criteria used to estimate MLD.

Anomalies of the MLD (MLD') at a given location (x, y) and time t are defined as

$$MLD'(x, y, t) = MLD(x, y, t) - \overline{MLD}(x, y, m), \tag{1}$$

where $\overline{MLD}$ is the climatological MLD value at location x, y and month m. Positive MLD' are defined here as deeper MLD than climatology. We use the Holte et al. (2017) climatological MLD that is produced by binning all MLD observations into 1° bins and computing the mean for each calendar month. It is important to note that the climatological MLD also includes measurements made inside of eddies. Therefore, any net influence of eddies on the mean MLD is included in the climatology. This generates significant changes in the average mixed layer, as shown by Hausmann et al. (2017) where they were able to conclude that eddies in the Southern Ocean deepen the average MLD by as much as 15 m. To test the effects of using a MLD climatology that includes eddies on the investigation presented here, we also compute climatologies using just profiles outside of eddies and compare to the seasonal evolution of the Holte et al. (2017) climatology in section 4.

To identify MLD within eddies for the global maps shown in section 3, we bin all observations of MLD occurring within a radial distance of L_s from the eddy center onto a global grid with horizontal spacing of 5° in longitude and 5° in latitude. Radial averages of MLD and MLD' presented in section 5 were constructed by first normalizing the radial distance of the profile location by the radius L_s and then subsequently computing bin averages with radial spacing of $0.3L_s$.

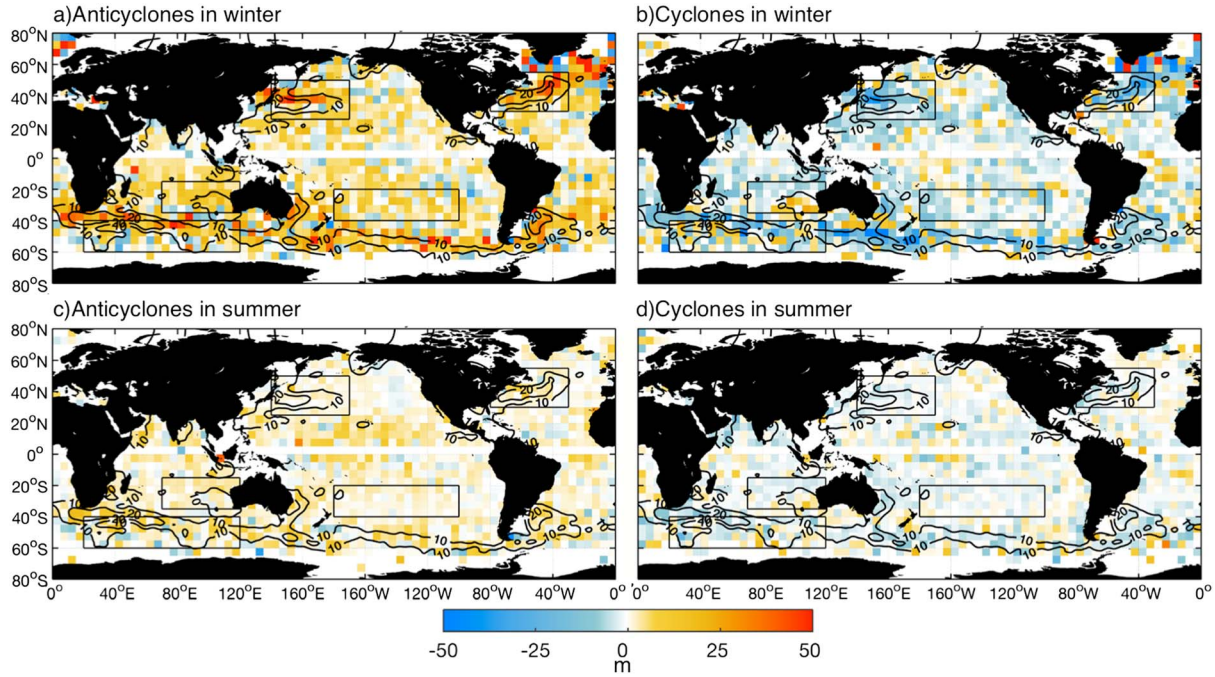

Figure 1. Eddy-induced MLD anomalies (*MLD*′) mapped to a global 5° grid. Observed *MLD*′ within L_s of the center of anticyclones in (a) winter and (c) summer in each hemisphere and cyclones in (b) winter and (d) summer in each hemisphere. Northern Hemisphere winter is defined as the period December through March and summer as the period June through September. Southern Hemisphere winter is defined as the period June through September and summer as the period December through March. The bounds of the regions analyzed in detail are as follows: North Atlantic Ocean 30°–55°N, 280°–330°E; North Pacific Ocean 25°–50°N, 140°–190°E; South Pacific 20°–40°S, 180°–260°E; south Indian Ocean 15°–35°S, 70°–120°E; Indian Ocean sector of the Southern Ocean 40°–60°S, 20°–120°E. Contours of eddy amplitude are overlaid. MLD = mixed layer depth.

3. Regional Variability of Eddy Influence on MLD

Detailed analysis of the seasonal and radial variability of MLD was conducted in four regions that were selected because they represent both boundary currents and areas of the open ocean that are characterized by both small and large magnitude *MLD*′ (see boxes in Figure 1). Globally, anticyclonic eddies deepen the MLD, resulting in positive *MLD*′ in nearly all regions, while cyclones shoal the mixed layer, generating negative *MLD*′ (Figure 1). Large-amplitude *MLD*′ are observed in the Southern Ocean along the Antarctic Circumpolar Current, as previously reported by Hausmann et al. (2017); in the North Atlantic (NA), in the eastern reaches of the Gulf Stream, the Greenland Sea, the Norwegian Sea, and the Barents Sea; and in the Brazil Malvinas Confluence; and the Agulhas Retroflection. These regions are all characterized by a very energetic mesoscale eddy field (see contours in Figure 1a), suggesting a robust relationship between the amplitude of eddies and the magnitude of their influence on *MLD*′. Along the equator, mesoscale ocean eddies are not identified in the SLA observations. In the near-equatorial regions, eddies are observed but are of small amplitude (see contours in Figure 1), thus resulting in small perturbations of MLD (see section 5).

4. Seasonal Variability of Eddy Influence on MLD

Maps of *MLD*′ computed separately in winter and summer indicate that eddy-induced *MLD*′ are larger in winter (Figures 1a and 1b) when compared to the summer (Figures 1c and 1d), which is consistent with previous regional investigations (Dufois et al., 2014; Gaube et al., 2013; Hausmann et al., 2017). To quantify the seasonal variability of MLD both within and outside of eddies, we constructed climatologies by fitting the seasonal cycle and its first harmonic to the observations in each of the regions indicated by the boxes in Figure 1.

During the boreal winter (January–February), MLD is at a maximum in both the NA and North Pacific (NP) with MLD in anticyclones reaching average depths of 170 m in the NA and 145 m in the NP (Figures 2a and 2b). During the boreal summer (June–July), the MLD shoals to average depths $<$ 20 m and eddy-induced perturbations are no longer detectable. Following these minima, MLD deepens throughout the boreal fall in both of these regions at a gradual rate of $\sim$ 10 m/month. This deepening is accelerated with the onset

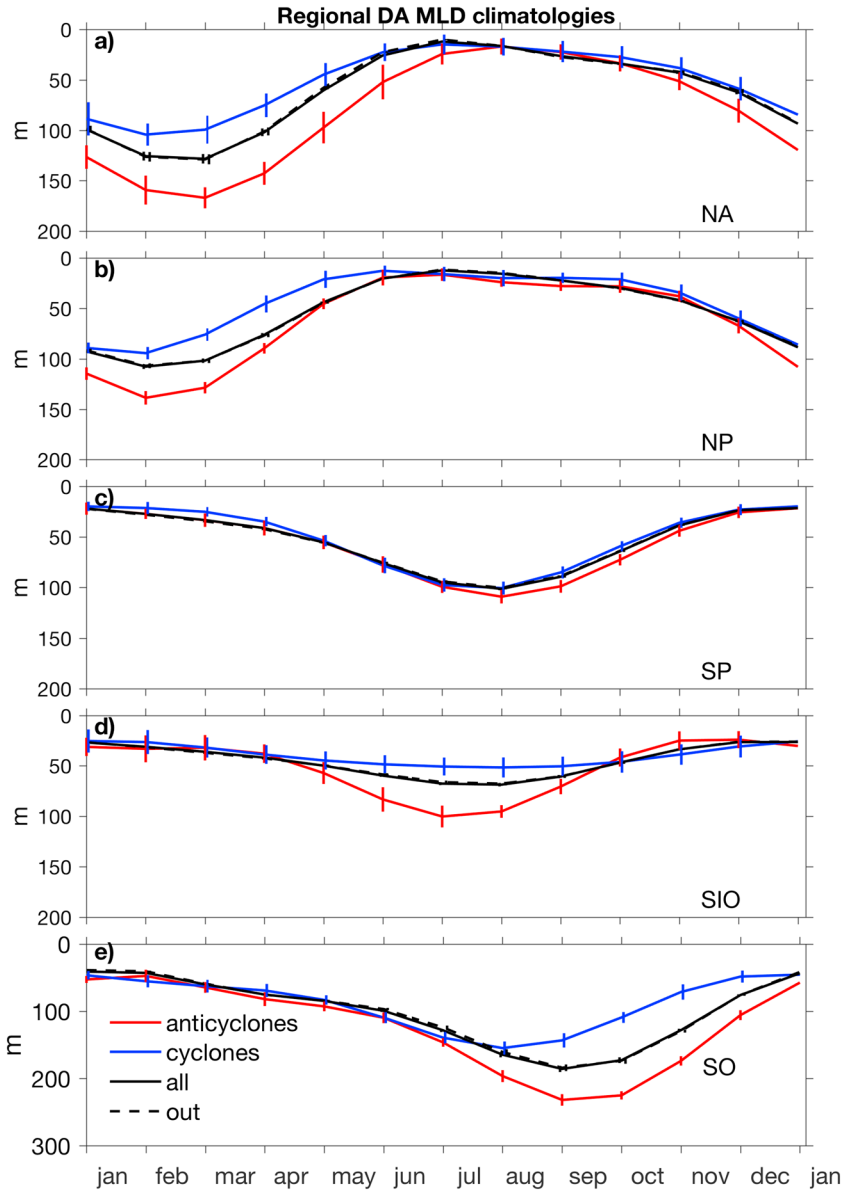

Figure 2. Seasonal cycle of mixed layer depth (MLD) in the North Atlantic Ocean (NA), North Pacific Ocean (NP), South Pacific (SP), south Indian Ocean (SIO), and Indian Ocean sector of the Southern Ocean (SO) regions defined in Figure 1. The cycles are created by least squares regression of the annual cycle and its first harmonic onto observations in anticyclones (red), cyclones (blue), outside of eddies (broken black curve), and all data (black curve). The standard error, computed as $\sigma/\sqrt{N}$, where σ is the standard deviation of all MLD observations during each calendar month and N is the number of MLD observations in each month, is indicated by the vertical lines.

of winter, and differences between MLD within and outside of eddies become statistically significant again starting in November in the NP and January in the NA.

In the South Pacific (SP) differences in MLD between cyclones and anticyclones are only significant in September and October (Figure 2c). In the south Indian Ocean (SI), the MLD in cyclones can only be distinguished from the background during June through August (Figure 2d). MLD in anticyclones is significantly deeper than outside of eddies in May thorough September. In the Indian Ocean sector of the Southern Ocean (SO), MLD is deeper within anticyclones from July through December (Figure 2e). Cyclones in the Indian Ocean sector of the SO analyzed here significantly shoal the MLD from the background values from August to November.

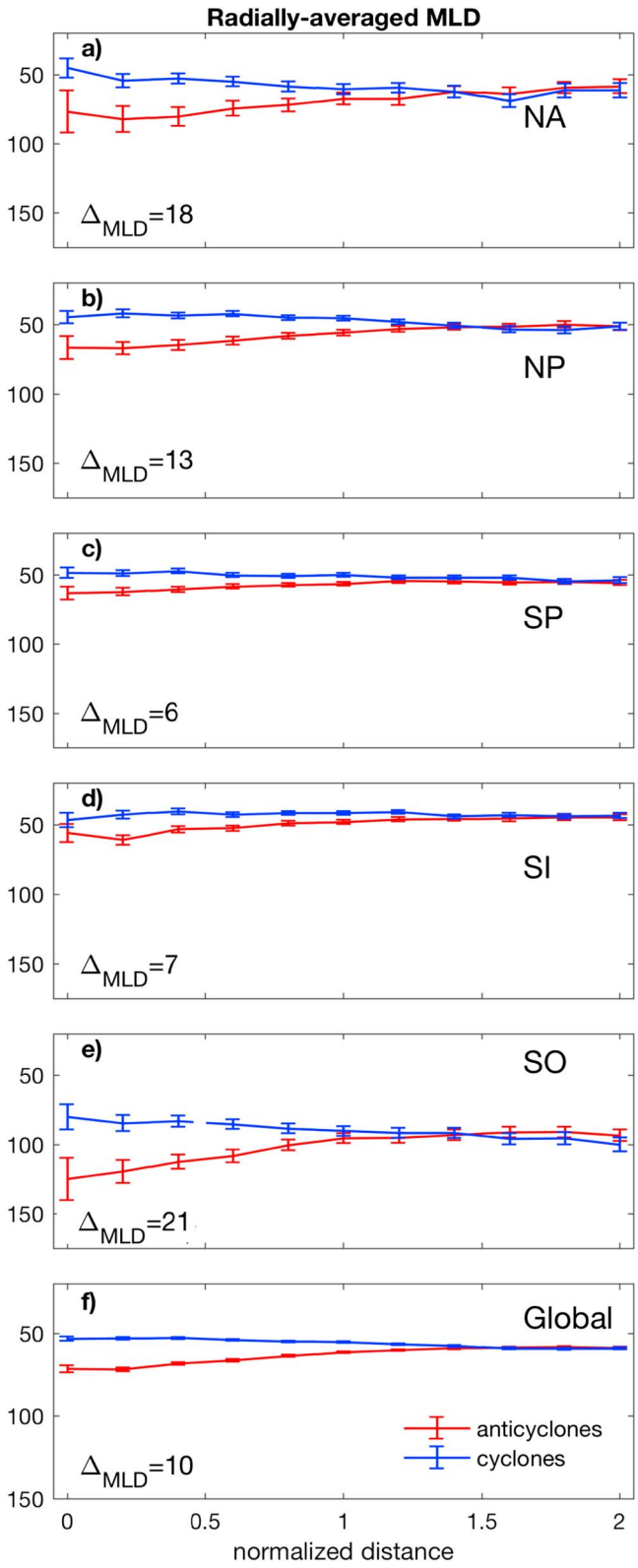

Figure 3. Winter radial averages of MLD in anticyclones (red) and cyclones (blue) for the five regions indicated in Figure 1 (a–e) and all eddies (f). The difference of MLD anomalies (*MLD′*) at the centers of anticyclones and cyclones is indicated as Δ_{MLD} in each panel of the left column. Error bars indicate the standard error of average MLD in each radial bin. MLD = mixed layer depth; NA = North Atlantic Ocean; NP = North Pacific Ocean; SP = South Pacific; SI = south Indian Ocean; SO = Indian Ocean sector of the Southern Ocean.

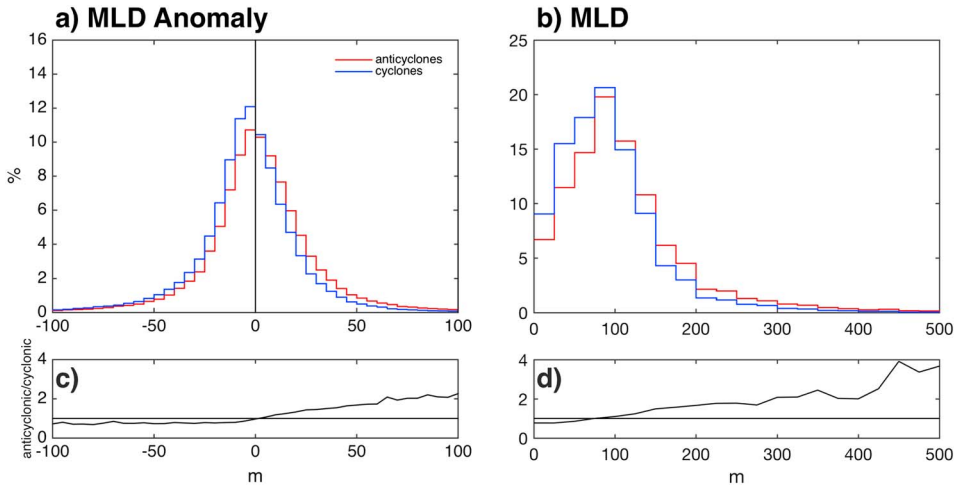

Figure 4. Histograms of global eddy-centric winter time *MLD′* (a) and MLD (b). The ratio of the red and blue lines in (a) and (b) are shown in (c) and (d). Anticyclones are shown in red and cyclones in blue. MLD = mixed layer depth.

5. The Structure of *MLD′* in Eddies

To investigate the spatial structure of winter MLD in eddies, we computed radial averages separately for each of the regions shown in Figure 1 and globally (Figure 3). Generally, the largest MLD perturbations occur near the center of eddies. In all regions MLD in anticyclones and cyclones are significantly different from each other throughout the eddy interiors ($r \leq L_s$), with the exception of the SI where MLD is not significantly different between eddies of either polarity in the region $0 \geq r < 0.2L_s$ (Figure 3d). Globally, MLD perturbations are larger in anticyclones when compared to cyclones.

Similar trends are evident in a global analysis. Positive (negative) *MLD′* (Figure 4a) and deeper (shallower) MLD (Figure 4b) tend to be associated with anticyclones and cyclones (red and blue lines, respectively). However, these tendencies are not exclusive; the distributions illustrate that anticyclones sometimes shallow the mixed layer, whereas cyclones sometimes deepen it. Ratios of the distributions reveal asymmetries in the response: anticyclones account for a larger share of positive *MLD′* and deep MLDs than cyclones do for negative *MLD′* and shallow MLD (Figures 4c and 4d).

The difference in MLD between anticyclones and cyclones (Δ_{MLD}) is largest in the SO, NA, and NP (Figures 3a, 3b, and 3e). These are regions of relatively large eddy amplitude (see contours in Figure 1a), suggesting that

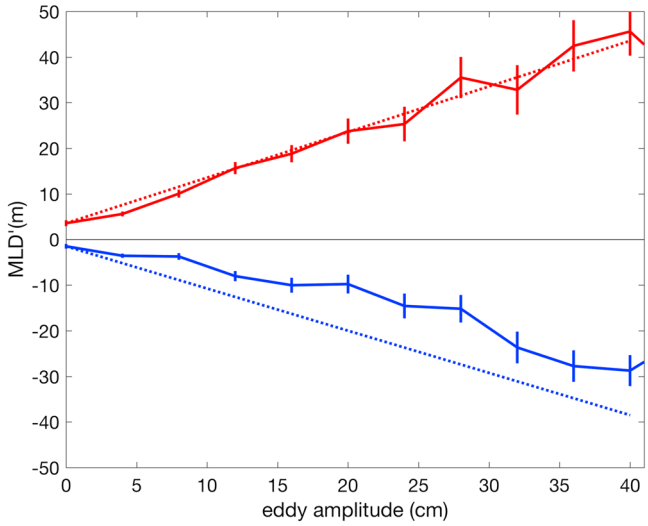

Figure 5. Average winter MLD anomalies (*MLD′*) as a function of eddy amplitude. The 100:1 cm/m relationship is indicated by the dashed lines. MLD = mixed layer depth.

MLD′ scales with eddy amplitude. Binning of wintertime *MLD*′ as a function of eddy amplitude reveals a nearly linear relationship (Figure 5). For anticyclones, this relationship is slightly steeper than 100:1, whereas for cyclones, this slope is slightly less steep.

6. Discussion and Conclusions

Mesoscale eddies modulate surface MLD globally. The magnitude of eddy-induced MLD anomalies is largest during the winter (Figure 2) in regions of large eddy amplitude (Figure 1). On average, MLD is deeper in anticyclones compared to cyclones. These differences may result from eddy effects on convective mixing associated with positive/negative SST anomalies generally observed in anticyclones/cyclones (i.e., Hausmann & Czaja, 2012; Gaube et al., 2015). In regions where the air temperature is lower than the SST, surface heat loss is expected to be higher in anticyclones and lower in cyclones, resulting in enhanced convection in anticyclones and suppressed convection in cyclones. This mechanism was first presented by Williams (1988) to explain observed differences in MLD in a pair of counter-rotating eddies in the NA. Identical twin experiments in cyclones and anticyclones confirmed that this differential heat flux could produce MLD anomalies similar in magnitude to those observed.

Globally, *MLD*′ in anticyclones are larger in magnitude when compared with cyclones. This asymmetry has been observed before in the SO (Hausmann et al., 2017) and the SI (Dufois et al., 2014; Gaube et al., 2013). Another possible mechanism that could result in this observed asymmetry is related to enhanced current shear at the base of the mixed layer in anticyclonic eddies. In a shipboard acoustic Doppler current profiler survey of a large anticyclone in the NA, Ledwell et al. (2008) reported enhanced shear at a depth of $\approx$ 40 m near the center of the eddy. Following the survey of this anticyclone, Greenan (2008) deployed a profiling acoustic velocity sensor on a drifting mooring which recorded enhanced shear events at the base of the mixed layer. Enhanced shear events observed by the profiling sensor revealed that such phenomena are complex and vary over time and as a function of distance from eddy center. Enhanced shear in anticyclones might result from the trapping of inertial gravity waves resulting from the modification of the effective planetary vorticity by the eddy. Kunze (1986) observed enhanced near-inertial motions associated with vertically propagating inertial gravity waves in the core of a warm-core Gulf Stream ring. These enhanced near-inertial motions observed by Kunze (1986), however, occur well below the surface mixed layer in a depth range of 300–500 m. Near the surface, inertial oscillations of passive Lagrangian surface drifters, which are drogued at 15 m and thus move with near-surface currents, have also been observed to be enhanced in anticyclones (Elipot et al., 2010).

As a result of the asymmetry in eddy effects on MLD, on average, eddies deepen mixed layers. The magnitude of this net deepening of MLD by eddies is expected to be largest in regions of large-amplitude eddies and deep winter mixing, as was shown by Hausmann et al. (2017) in the SO. This integrated effect needs to be included, or parameterized, in ocean models in order to correctly reproduce eddy effects on near-surface mixing and biogeochemical cycling (e.g., Harrison et al., 2018).

These mesoscale MLD anomalies may modulate biogeochemical cycling via numerous mechanisms. For example, the average incident photosynthetically active radiation in mixed layers of anticyclones would be lower than that of cyclones of the same SLA amplitude as a result of the exponential decay of light with depth. Deeper MLDs may result from enhanced mixing, which can lead to enhanced nutrient fluxes in regions where the nutricline is collocated with the base of the mixed layer. Adding to these "bottom-up" controls on production, mesoscale modulation of mixing in anticyclones could act to decouple grazers and phytoplankton by reducing encounter rates as a result of dilution (Behrenfeld, 2010; Behrenfeld & Boss, 2014). The relationship between eddy amplitude and MLD could be used as a basis for parameterizing the effects of mesoscale eddies on MLD and biogeochemical cycling (e.g., Harrison et al., 2018).

Acknowledgments
This project was supported by NASA grants NNX13AE47G and NNX16AH9G. This manuscript was improved as a result of helpful discussions with Jeffery Early, Johnathan Lilly, and Eric Kunze of Northwest Research Associates. D. J. M. also gratefully acknowledges support of the National Science Foundation. The eddy data set used here is distributed by AVISO at https://www.aviso.altimetry.fr/en/data/products/value-added-products/global-mesoscale-eddy-trajectory-product.html. The MLD data can be accessed at http://mixedlayer.ucsd.edu.

References

Behrenfeld, M. J. (2010). Abandoning Sverdrup's critical depth hypothesis on phytoplankton blooms. *Ecology*, *91*(4), 977–989.
Behrenfeld, M. J., & Boss, E. S. (2014). Resurrecting the ecological underpinnings of ocean plankton blooms.
Chelton, D., Gaube, P., Schlax, M., Early, J., & Samelson, R. (2011). The influence of nonlinear mesoscale eddies on near-surface oceanic chlorophyll. *Science*, *334*(6054), 328–332.
Chelton, D., & Schlax, M. (2016). The "growing method" of eddy identification and tracking in two and three dimensions.
Chelton, D., Schlax, M., & Samelson, R. (2011). Global observations of nonlinear mesoscale eddies. *Progress in Oceanography*, *91*(2), 167–216.
Dawson, H. R. S., Strutton, P. G., & Gaube, P. (2018). The unusual surface chlorophyll signatures of Southern Ocean eddies. *Journal of Geophysical Research: Oceans*, *123*, 6053–6069. https://doi.org/10.1029/2017JC013628
Dewar, W., & Flierl, G. (1987). Some effects of the wind on rings. *Journal of Physical Oceanography*, *17*(10), 1653–1667.

Dufois, F., Hardman-Mountford, N. J., Greenwood, J., Richardson, A. J., Feng, M., Herbette, S., & Matear, R. (2014). Impact of eddies on surface chlorophyll in the south Indian Ocean. *Journal of Geophysical Research: Oceans*, *119*, 8061–8077. https://doi.org/10.1002/2014JC010164

Dufois, F., Hardman-Mountford, N. J., Greenwood, J., Richardson, A. J., Feng, M., & Matear, R. J. (2016). Anticyclonic eddies are more productive than cyclonic eddies in subtropical gyres because of winter mixing. *Science Advances*, *2*(5), e1600282.

Elipot, S., Lumpkin, R., & Prieto, G. (2010). Modification of inertial oscillations by the mesoscale eddy field. *Journal of Geophysical Research*, *115*, C09010. https://doi.org/10.1029/2009JC005679

Frenger, I., Münnich, M., & Gruber, N. (2018). Imprint of Southern Ocean mesoscale eddies on chlorophyll. *Biogeosciences*, *15*(15), 4781–4798.

Gaube, P., Chelton, D., Samelson, R., O'Neill, L., Schlax, M., & Hoecker-Martinex, M. (2015). Satellite observations of mesoscale eddy-induced Ekman pumping. *Journal of Physical Oceanography*, *45*, 104–132.

Gaube, P., Chelton, D., Strutton, P., & Behrenfeld, M. (2013). Satellite observations of chlorophyll, phytoplankton biomass and Ekman pumping in nonlinear mesoscale eddies. *Journal of Geophysical Research: Oceans*, *118*, 6349–6370. https://doi.org/10.1002/2013JC009027

Greenan, B. J. (2008). Shear and Richardson number in a mode-water eddy. *Deep Sea Research Part II*, *55*(10), 1161–1178.

Harrison, C. S., Long, M. C., Lovenduski, N. S., & Moore, J. K. (2018). Mesoscale effects on carbon export: A global perspective. *Global Biogeochemical Cycles*, *32*(4), 680–703. https://doi.org/10.1002/2017GB005751

Hausmann, U., & Czaja, A. (2012). The observed signature of mesoscale eddies in sea surface temperature and the associated heat transport. *Deep Sea Research Part I*, *70*, 60–72.

Hausmann, U., McGillicuddy, D. J., & Marshall, J. (2017). Observed mesoscale eddy signatures in Southern Ocean surface mixed-layer depth. *Journal of Geophysical Research: Oceans*, *122*, 617–635. https://doi.org/10.1002/2016JC012225

Holte, J., & Talley, L. (2009). A new algorithm for finding mixed layer depths with applications to Argo data and subantarctic mode water formation. *Journal of Atmospheric and Oceanic Technology*, *26*(9), 1920–1939.

Holte, J., Talley, L. D., Gilson, J., & Roemmich, D. (2017). An Argo mixed layer climatology and database. *Geophysical Research Letters*, *44*, 5618–5626. https://doi.org/10.1002/2017GL073426

Joyce, T., Patterson, S., & Millard, R. (1981). Anatomy of a cyclonic ring in the drake passage. *Deep Sea Research*, *28*(11), 1265–1287.

Klein, P., Treguier, A.-M., & Hua, B. L. (1998). Three-dimensional stirring of thermohaline fronts. *Journal of Marine Research*, *56*(3), 589–612.

Kunze, E. (1986). The mean and near-inertial velocity fields in a warm-core ring. *Journal of Physical Oceanography*, *16*, 1444–1461.

Ledwell, J., McGillicuddy, D. Jr, & Anderson, L. (2008). Nutrient flux into an intense deep chlorophyll layer in a mode-water eddy. *Deep Sea Research Part II*, *55*(10-13), 1139–1160.

Schmitt, R. W., & Olson, D. B. (1985). Wintertime convection in warm-core rings: Thermocline ventilation and the formation of mesoscale lenses. *Journal of Geophysical Research*, *90*(C5), 8823–8837.

Scott, R. B., & Wang, F. (2005). Direct evidence of an oceanic inverse kinetic energy cascade from satellite altimetry. *Journal of Physical Oceanography*, *35*(9), 1650–1666.

Song, H., Long, M. C., Gaube, P., Frenger, I., Marshall, J., & McGillicuddy, D. J. Jr (2018). Seasonal variation in the correlation between anomalies of sea level and chlorophyll in the Antarctic Circumpolar Current. *Geophysical Research Letters*, *45*, 5011–5019. https://doi.org/10.1029/2017GL076246

The Ring Group (1981). Gulf stream cold-core rings: Their physics, chemistry, and biology. *Science*, *212*(4499), 1091.

Vastano, A. C., Schmitz, J. E., & Hagan, D. E. (1980). The physical oceanography of two rings observed by the cyclonic ring experiment. Part I: Physical structures. *Journal of Physical Oceanography*, *10*(4), 493–513.

Waite, A., Pesant, S., Griffin, D., Thompson, P., & Holl, C. (2007). Oceanography, primary production and dissolved inorganic nitrogen uptake in two Leeuwin Current eddies. *Deep Sea Research Part II*, *54*(8-10), 981–1002.

Williams, R. (1988). Modification of ocean eddies by air-sea interaction. *Journal of Geophysical Research*, *93*, 15,523–15,533. https://doi.org/10.1029/JC093iC12p15523

Williams, S., Petersen, M., Bremer, P.-T., Hecht, M., Pascucci, V., Ahrens, J., et al. (2011). Adaptive extraction and quantification of geophysical vortices. *IEEE Transactions on Visualization and Computer Graphics*, *17*(12), 2088–2095.